ACS ES&T Air

pubs.acs.org/estair

Article

Photochemical Cloud Processing of Water-Soluble Organic Gases Produced by Aqueous-Phase Photooxidation of α-Pinene, d-Limonene, and Toluene

Matthew L. Zaragoza, Lisa M. Wingen, Sergey A. Nizkorodov,* and Annmarie G. Carlton*

Cite This: ACS EST Air 2026, 3, 1811−1821

Read Online

ACCESS | Metrics & More | Article Recommendations | Supporting Information

ABSTRACT: Ambient water-soluble organic gases (WSOGs) are photochemically processed in atmospheric waters, which contributes to aqueous secondary organic aerosol (aqSOA). Chemical characterization of this atmospheric pathway has not been undertaken for monoterpene or aromatic oxidation products. In this work, gas-phase α-pinene, d-limonene, and toluene were oxidized via O_3- and •OH-initiated reactions. Resulting water-soluble oxidation products were collected using a mist chamber, in which WSOGs were scrubbed by aqueous droplets. WSOG samples were then subjected to aqueous-phase photooxidation to quantify aqSOA mass yields and characterize aqSOA chemical composition. AqSOA particle mass concentrations and O/C ratios increased with aqueous-phase photooxidation time for monoterpene WSOGs, while only marginal increases were observed for toluene WSOGs. Mass spectra for α-pinene WSOGs showed an abundance of small carboxylic acids (C_1−C_4) and monomeric (C_7− C_{10}) carbonyls formed during the aqueous-phase photooxidation. The α-pinene WSOGs exhibited a distinct molecular composition and underwent different photochemical processes when contrasted with water-soluble organic particles (WSOPs) from the gas-phase oxidation of α-pinene. These results underscore the need for chemical-level characterization of monoterpene-derived WSOGs to quantitatively evaluate their potential contribution to the global atmospheric aqSOA burden.

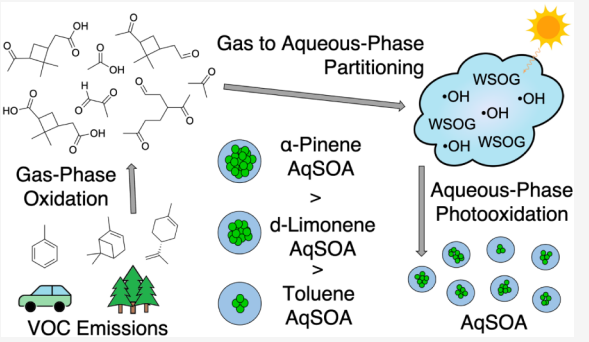

KEYWORDS: *aqueous-phase photooxidation, aqueous secondary organic aerosol (aqSOA), cloud processing, mist chamber, multiphase chemistry*

1. INTRODUCTION

The oxidation of volatile organic compounds (VOCs) in the atmosphere forms oxidized organic compounds, including water-soluble organic gases (WSOGs), that contribute to secondary organic aerosol (SOA) through physical and reactive uptake in existing particles or droplets.[1,2] Tropospheric WSOGs are primarily small, polar carbonyl compounds and carboxylic acids. Formic and acetic acids are the most abundant carboxylic acids, found widely in the atmosphere in both urban and remote regions.[3−7] Dicarboxylic acids, such as oxalic and malonic acids, are also abundant.[2,8−11] Carboxylic acids are routinely observed in cloud and fogwater[12−15] as well as in the particle phase, in larger amounts than predicted by their vapor pressure.[16−18]

SOA generated from gas-phase reaction pathways (gasSOA) has been studied through the oxidation of a variety of biogenic and anthropogenic VOCs, including isoprene, α-pinene, d-limonene, and toluene.[19−22] Isoprene, α-pinene, toluene, and biomass burning emissions all exhibit higher SOA mass yields from aqueous pathways (aqSOA) than gasSOA.[23−25] Isoprene and aromatic oxidation products, such as glyoxal, methylglyoxal, glycolaldehyde, and pyruvic acid, are well-established aqSOA precursors.[26−32] Monoterpene oxidation products, including pinonic, pinic, and limononic acids, are also reported to form aqSOA.[33−37] In addition to laboratory experiments, ambient WSOG samples have been shown to form aqSOA through aqueous-phase photooxidation, in which several water-soluble precursors were proposed and tentatively characterized.[38,39] Water-soluble organic particles (WSOPs) are gasSOA particles that partition into the aqueous phase. WSOPs may undergo further processing in the aqueous phase to generate aqSOA, but only the newly generated SOA in the aqueous phase is considered aqSOA, whereas all SOA produced from WSOG aqueous-phase processing is considered aqSOA.

Atmospheric liquid water is a readily abundant partitioning medium in the troposphere and exists primarily in the form of

Received: February 4, 2026
Revised: May 20, 2026
Accepted: May 21, 2026
Published: June 4, 2026

https://doi.org/10.1021/acsestair.6c00044
ACS EST Air 2026, 3, 1811−1821

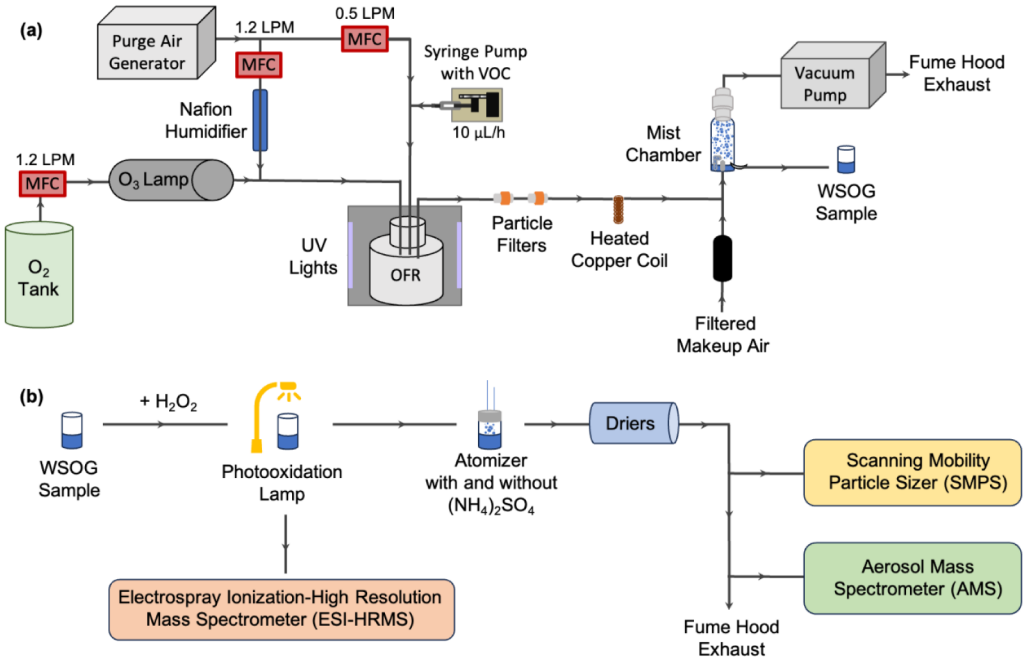

Figure 1. (a) Diagram of WSOG sample generation from the OFR. Samples were collected in the mist chamber for aqueous-phase photooxidation and characterization. MFC = mass flow controller; OFR = oxidation flow reactor. (b) Diagram of WSOG sample aqueous-phase photooxidation and characterization. After mist chamber WSOG collection, samples were separated into separate aliquots for SMPS, AMS, and ESI-HRMS data collection.

cloud droplets and aerosol liquid water (ALW). Cloud droplets are more dilute than ALW but still contain a myriad of species, including organic acids, aromatics, terpene derivatives, inorganic ions, and heteroatom-containing compounds.[13,40−44] The predominant oxidant in atmospheric aqueous environments is the •OH radical,[45,46] which has been modeled to be primarily responsible for the production of aqSOA.[47] Liquid water in atmospheric environments displays average mass concentrations two to three times higher than dry organic aerosol mass concentrations.[48,49] Thus, aqueous pathways are predicted to contribute substantially to total SOA mass in some locations.[2,49−51] However, the composition of atmospherically relevant WSOGs, their aqueous processing mechanisms, and their efficiency at generating aqSOA are all poorly constrained.[10,47]

In this study, an oxidative flow reactor (OFR) was used to oxidize α-pinene, d-limonene (referred to as limonene hereafter), and toluene individually in the gas phase. The monoterpenes α-pinene and limonene have high global emission rates,[52] and toluene emissions are important in urban environments.[53−55] WSOG oxidation products were collected by neat water droplets in a mist chamber to simulate the passing of an air parcel containing VOC oxidation products through a cloud. Mist chambers are known to rapidly partition WSOGs into the aqueous phase and facilitate the collection of trace levels of WSOGs.[56,57] WSOG samples were photooxidized in the aqueous phase to generate aqSOA. A Scanning Mobility Particle Sizer (SMPS), Aerosol Mass Spectrometer (AMS), and Electrospray Ionization-High Resolution Mass Spectrometer (ESI-HRMS) were used to quantify and chemically characterize aqSOA. The aqueous-phase photooxidation of WSOGs from α-pinene, limonene, and toluene was found to produce highly oxidized aqSOA in all three cases, with α-pinene WSOGs producing the highest aqSOA yield. The results from this study suggest that monoterpene-derived WSOGs can serve as a global source of aqSOA in the atmosphere.

2. METHODS

2.1. SOA Generation

A home-built oxidation flow reactor (OFR; see Veghte et al. for more details)[58] produced gas-phase oxidation products by the O_3- and •OH-initiated oxidation of VOCs (Figure 1a). The OFR consisted of an 8 L quartz vessel where the VOC and oxidants were mixed. Two 254 nm lamps generated •OH radicals by the photolysis of O_3 in the presence of water vapor. The overall gas flow (2.4 L/min) through the OFR consisted of 1.2 L/min O_2 flow (UHP grade, Airgas) that passed through an O_3-generating lamp, 0.7 L/min humidified (100% RH) air, and 0.5 L/min dry air, which contained a VOC. The estimated residence time inside the OFR was 3.3 min. A syringe pump delivered the VOC at a rate of 10 μL/h into the VOC air flow. The RH of the OFR was ∼30%, the measured O_3 mixing ratio (in the absence of added VOC) was ∼12 ppm, and the calculated steady-state mixing ratio of VOC (in the absence of O_3) was 8.67−13.2 ppm depending on the VOC. The monoterpenes were primarily oxidized by •OH, which constituted ∼66% and ∼83% of the α-pinene and limonene gas-phase oxidation, respectively. Toluene was almost exclusively oxidized by •OH (see section S3 for more details). The outflow from the OFR (at 2.4 L/min) passed through two 0.2 μm Teflon filters in series to remove particles. Gaseous oxidation products then entered heated (∼110 °C) copper tubing (2.7 m) to scrub residual O_3 from the sample. The efficiency of the scrubber was measured in a separate experiment, where it was found to lower the O_3 mixing ratio from ∼12 ppm to less than 0.1 ppm.

2.2. Mist Chamber

Clean air mixed with gas-phase oxidation products from the OFR flowed through the mist chamber at a flow rate of ∼29.3 L/min. WSOGs partitioned from the gas phase into the aqueous phase via droplets of the mist chamber (see Figure S1).[56] WSOGs derived from the gas-phase photooxidation of a specific VOC are referred to as VOC WSOGs within this work. Since the flow from the OFR was much smaller than the optimal mist chamber flow, clean makeup flow

https://doi.org/10.1021/acsestair.6c00044
ACS EST Air 2026, 3, 1811−1821

of lab air, passing through two HEPA particle filters and three charcoal cartridge filters, was added in series to the OFR prior to the mist chamber (this air was verified to contain no WSOGs in preliminary experiments). The HEPA filters were added upstream of the charcoal denuders to prevent gaseous siloxane contamination[59] from entering the mist chamber apparatus. Purified water (Thermo Scientific GenPure Pro UV 18.2 MΩ cm) was used as the working fluid in the chamber. A syringe pump (Tricontinent C-Series) transferred the neat water into and dissolved WSOGs out of the mist chamber reservoir. A hydrophobic membrane filter (TISCH Scientific PTFE Membrane Filter, 1.0 μm pore size, 47 mm diameter) minimized water loss at the mist chamber exit. Some evaporative loss still occurred, with an evaporation rate that varied with RH.[4,60] Droplets were generated with 15.0 mL of neat water and misted for 5 min. In this experimental setup, 13.8 mL of water was retained in the mist chamber after 5 min of misting, indicating an evaporative loss rate of 0.24 mL/min. OFR oxidation occurred continuously while a mist chamber cycle was repeatedly collected every 7 min (1 min water injection, 5 min sampling, and 1 min WSOG sample removal). This mist chamber cycle was repeated until a total of 200.0 mL was collected in a clean glass jar. Sample aliquots were divided into four 50.0 mL batches for AMS and SMPS analysis. Three replicates were collected for each VOC. An additional 40.0 mL batch of α-pinene WSOG sample was collected for ESI-HRMS analysis.

2.3. Aqueous-Phase Photooxidation

Aqueous WSOG samples were photooxidized to simulate reactions in cloud droplets. To accomplish this, 0.045 M H_2O_2 (30% ACS grade) was added to WSOG samples, and solutions were irradiated in open air by a 254 nm pen-ray lamp (see Figure S2) to generate •OH radicals. For AMS and SMPS analysis (described below), multiple identical WSOG samples were irradiated at 0, 30, 60, and 90 min. For the α-pinene experiments, particulate matter exiting the OFR that deposited on Teflon filters was extracted to characterize water-soluble organic particles (WSOPs) for comparison to WSOGs. Approximately 1.0 mg of α-pinene SOA was collected on the filter paper and dissolved in 40.0 mL of neat water for 15 min to extract WSOPs, which constitute the majority of α-pinene-derived SOA material.[61] Extracted WSOP samples were subjected to the same H_2O_2 and UV radiation as the WSOG samples. For ESI-HRMS analysis, α-pinene WSOG and WSOP samples were photooxidized in the aqueous phase from 0 to 90 min in increments of 10 min.

In a separate calibration experiment, terephthalic acid was used in place of WSOGs as an •OH-trapping compound to measure and test the steady-state concentration of •OH radicals present in solution for this experimental setup. A steady-state •OH concentration of 1.7×10^{-13} M was calculated for WSOG solutions in the employed experimental design (see SI section 4.1 and section 4.2). After the longest aqueous-phase photooxidation exposure of 90 min, 99% H_2O_2 was estimated to remain in solution, consistent with the steady-state assumption (see SI section 4.3). For this •OH concentration, 90 min of aqueous-phase photooxidation in the experiment is equivalent to ~25 h of cloud processing time (see SI section 4.4). This value approximates many cloud cycles as an air parcel undergoes vertical transport and entrainment through cloud environments.

2.4. Sample Characterization

Aqueous samples were examined using SMPS, AMS, and ESI-HRMS instruments after aqueous-phase photooxidation (Figure 1b). AqSOA samples were individually atomized at 2.0 L/min and passed through a set of dryers before entering an AMS (0.1 L/min sampling flow) and an SMPS (0.3 L/min sampling flow). Three aqSOA samples were analyzed for each VOC with both instruments. SMPS measurements were used to determine particle mass concentrations and calculate aqSOA yields as a function of the aqueous photooxidation time. Variability among measured mass concentrations for the same VOC was attributed to inconsistencies in the OFR output, as observed in preliminary total organic carbon (TOC) analyzer measurements. It is important to note that the RH in the SMPS sheath flow was 15−40%, and the particles were not fully dried; however, the water content can be expected to be low for pure organic particles. The dried particle sizes were too small for AMS measurements, so after SMPS measurements were complete, 0.1 mM of ammonium sulfate (AS) was added to improve the AMS particle detection efficiency. The percent mass of the sample within the AMS measurable diameter range (greater than 70 nm) increased from approximately 5% to 50% after adding AS, as determined from preliminary SMPS measurements (see SI section 10 for more details).

Direct infusion into a Q Exactive Plus electrospray ionization high-performance Orbitrap mass spectrometer (ESI-HRMS) was used for the chemical characterization of aqueous-phase α-pinene WSOG photooxidation products. Direct infusion samples were averaged over 2 min in both positive ion (ESI(+)) and negative ion (ESI(−)) modes. ESI(−) ions were assumed to form only by deprotonation. ESI(+) ions were assumed to form of either a sodium ion or proton addition. Species will be referred to by their neutral formulas, and tentative identities are provided in parentheses in the results section. Ion fragments are still formed using a soft ionization technique such as ESI, so some of the formulas may correspond to fragments of larger molecules.

2.5. Mass Yield Calculations

Mass yields of aqSOA were calculated in two ways, with each method employing values at the different aqueous photooxidation times (Table 1). The first yield (Y_1) represents the mass fraction of captured WSOGs that became aqSOA after aqueous-phase photooxidation and atomization. The second yield (Y_2) is defined as the mass fraction of the initial VOC that was ultimately converted into aqSOA after gas-phase VOC oxidation, mist chamber sampling of WSOGs, aqueous-phase photooxidation, and atomization of the solution. Y_2 is more akin to the yields traditionally calculated in smog chamber experiments. Calculations for Y_1 and Y_2 are provided in SI section 5.

Table 1. aqSOA Yields for All Three Aqueous-Phase Photooxidation Times[a]

Mass Yield	α-Pinene aqSOA (%)	Limonene aqSOA (%)	Toluene aqSOA (%)
30 min			
Y_1	8.7 ± 4.4	7.5 ± 3.8	2.1 ± 1.1
Y_2	1.4 ± 0.5	1.2 ± 0.2	0.28 ± 0.11
60 min			
Y_1	10 ± 5	8.1 ± 4.1	3.2 ± 1.6
Y_2	1.7 ± 0.6	1.4 ± 0.3	0.45 ± 0.02
90 min			
Y_1	11 ± 5	7.6 ± 3.8	2.9 ± 1.4
Y_2	1.9 ± 0.4	1.4 ± 0.4	0.42 ± 0.13

[a]Y_1 represents the mass fraction of dissolved WSOG mass that was photooxidized to aqSOA. Y_2 represents the mass fraction of VOC that entered the OFR, partitioned into the WSOG sample, and was photooxidized to aqSOA.

3. RESULTS

3.1. Mass Concentration and Yield

The amount of aqSOA mass produced from each WSOG system generally increased with aqueous photooxidation time (Figure 2). For example, the measured mass concentrations for α-pinene aqSOA were approximately 3 $\mu g/m^3$ and increased to nearly 15 $\mu g/m^3$ at 90 min of aqueous-phase photooxidation (Figure 2a) in bulk solution. The monoterpene aqSOA had significantly higher mass concentrations after 90 min of aqueous-phase photooxidation compared to toluene aqSOA. WSOGs generated from the toluene experiments exhibited lower observed TOC concentrations (Figure S5) relative to the studied monoterpene systems. This observation is

https://doi.org/10.1021/acsestair.6c00044
ACS EST Air 2026, 3, 1811−1821

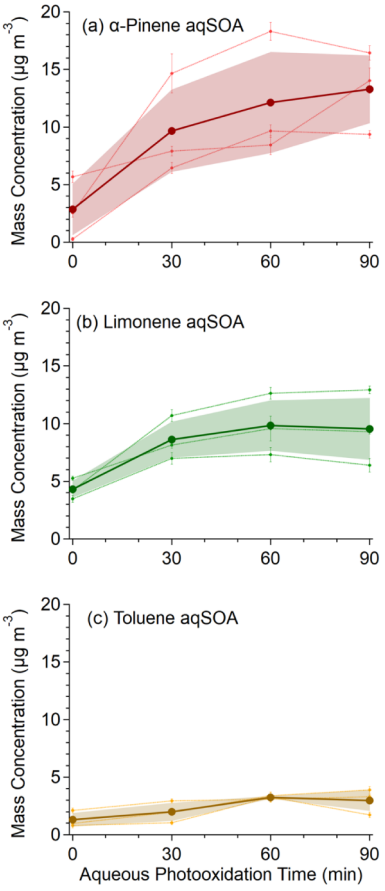

Figure 2. Mass concentration from SMPS measurements for α-pinene aqSOA (a), limonene aqSOA (b), and toluene aqSOA (c). Each type of WSOG sample had three separate trials, represented by the smaller dashed lines, with five measurements per trial. The bolded line represents the average of the three trials. Error bars and shading indicate one standard deviation.

consistent with toluene oxidation products having lower Henry's law constants and smaller molecular weights relative to the studied monoterpene oxidation products,[62] which would reduce partitioning into the aqueous phase and subsequent aqSOA formation. AqSOA observed prior to aqueous-phase photooxidation likely resulted from reaerosolization of dissolved WSOGs after storage, consistent with previous laboratory observations of aqSOA under dark conditions from WSOG precursors.[63−67] For both limonene and toluene systems, aqSOA mass concentrations plateaued by 60 min of aqueous-phase photooxidation, with measurements from 60 to 90 min remaining within one standard deviation. Similar maxima in aqSOA mass have been observed in aqueous-phase photooxidation experiments of ambient cloudwater samples[14,68] and are attributed to competing functionalization, fragmentation, and evaporation rates.[14,68]

The aqSOA mass yields for both Y_1 (aqSOA mass normalized by the initial WSOG mass) and Y_2 (aqSOA mass normalized by the initial VOC mass) were highest for α-pinene, with values of 11 ± 5% and 1.9 ± 0.4%, respectively (Table 1). Initial WSOG mass was determined through TOC measurements (see Sections S5 and S6 for more details). Quantitative data for comparison to other studies are relatively sparse, but Y_1 for aqSOA was determined to be ∼40% for pinonic acid using an •OH concentration of 1.7×10^{-13} M after 120 min[33] and ∼50% for glycolaldehyde using an •OH concentration of $\sim 10^{-12}$ M after 70 min.[31] The Y_2 value for isoprene aqSOA was modeled to range from 0.3−1.1%.[69] The isoprene aqSOA yields predicted by Ervens et al.[69] are smaller than the Y_2 values measured here for α-pinene and limonene aqSOA, which is qualitatively consistent with the larger molecular weights of WSOGs generated from monoterpene (C_{10} compounds) oxidation versus isoprene (C_5 compound) oxidation. It should be noted that in the Ervens et al.[69] (2008) modeling study, gas- and aqueous-phase oxidation occurred concurrently, while in these experiments, the processes are sequential.

3.2. Elemental Analysis

There was a clear increase in both AMS-derived average carbon oxidation state (OSc) and oxygen-to-carbon (O/C) ratio with aqueous photooxidation time for aqSOA samples in all three VOC systems (Figure 3). Both O/C ratio and OSc

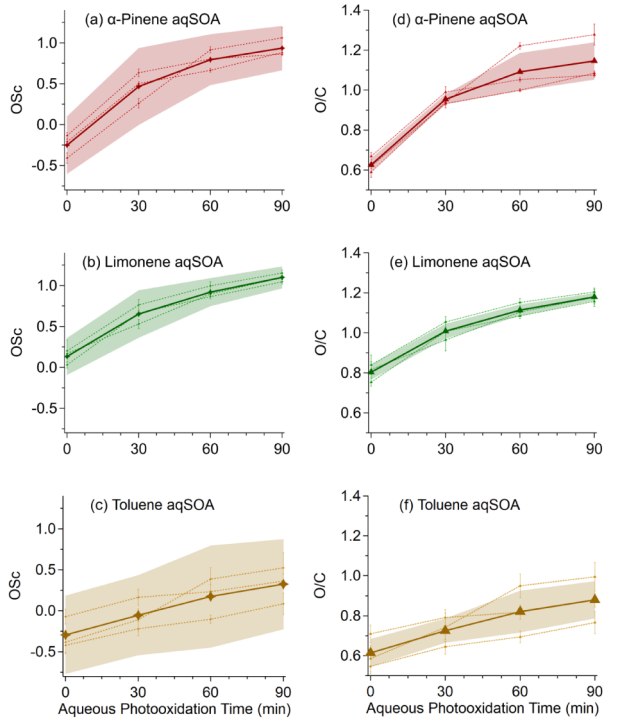

Figure 3. Average oxidation state of carbon (OSc) and oxygen-to-carbon ratio (O/C) for α-pinene aqSOA (**a, d**), limonene aqSOA (**b, e**), and toluene aqSOA (**c, f**) over the course of aqueous-phase photooxidation. The left panels show OSc, and the right panels show O/C ratios measured by the AMS. Each type of WSOG sample had three separate trials, represented by the smaller dashed lines, with five measurements per trial. The bolded line represents the average of the three trials. Error bars and shading indicate one standard deviation.

measurements are reported because O/C ratios are more commonly recorded in the literature, but OSc is less affected by dehydration and hydration reactions and is therefore a better proxy to understand the properties of aqSOA.[70] OSc reached 0.94 for α-pinene aqSOA, 1.1 for limonene aqSOA, and 0.32 for toluene aqSOA. The O/C ratios for aqSOA ranged from 0.63−1.1 for α-pinene, 0.80−1.2 for limonene, and 0.61−0.88 for toluene. Atomized cloud water samples collected at Whistler, British Columbia, Canada, and Mt. Tai, China, exhibited O/C ratios between 0.35−0.55 in AMS analysis,[14,38] lower than the values measured here. After

https://doi.org/10.1021/acsestair.6c00044
ACS EST Air 2026, 3, 1811−1821

comparable amounts of aqueous-phase photooxidation, O/C ratios of the Whistler and Mt. Tai samples increased to 0.4−1, consistent with an increase in the average O/C ratio with aqueous photooxidation time as observed here. Several studies recorded a decrease in O/C ratios after extended periods of aqueous-phase photooxidation,[14,68] thought to be caused by the evaporation of highly oxidized compounds (such as formic acid) from aqueous samples. We note that evaporation would be suppressed during the aqueous-phase photooxidation of our bulk solutions, but volatile products would evaporate during the atomization step.

In a separate AMS experiment, the O/C ratios of gas-phase oxidized particles for each VOC were measured (see SI section 10). The oxidized monoterpene particle O/C ratios were determined to be 0.49 ± 0.01 for α-pinene and 0.53 ± 0.01 for limonene, which is in agreement with previous literature[38,71,72] but lower than their respective WSOG O/C ratios (0.63 and 0.80). Lee et al.[38] examined the aqueous-phase photooxidation of α-pinene oxidation products, including both gases and particles, as a function of f_{44}/f_{43} ratio (which is a proxy for O/C ratio) by comparing the CO_2^+ fragment (nominal m/z 44) to the $C_2H_3O^+$ fragment (nominal m/z 43).[38] Lee et al.[38] observed an increase in f_{44}/f_{43} from ∼0.48 to ∼3.2 from the aqueous-phase photooxidation of α-pinene SOA generated in a flow tube reactor. The f_{44}/f_{43} ratio for the α-pinene WSOGs in this study rose from 2.5 to 3.3. This comparison indicates that WSOGs were initially more oxidized than WSOPs, but after 90 min of aqueous-phase photooxidation, the WSOPs and WSOGs had a more similar extent of oxidation. In contrast, toluene gas-phase oxidation product particles were determined in a separate AMS experiment to have an O/C ratio of 0.80 ± 0.01, which was in agreement with the literature[73] and higher than the toluene WSOG O/C ratio (0.61). Toluene WSOGs had an O/C ratio similar to α-pinene WSOGs prior to aqueous-phase photooxidation, but toluene aqSOA only reached an O/C ratio of 0.88 in comparison to α-pinene aqSOA, which obtained an O/C ratio of 1.1.

AMS-identified fragments provide evidence for increasing O/C ratios during aqueous-phase photooxidation through progressive functionalization of aqSOA components (Figure 4). The CO_2^+ fragment, commonly associated with highly oxidized carboxylic acid functional groups,[74] increased with aqueous photooxidation time for the monoterpene systems, whereas smaller changes were observed for toluene aqSOA. In contrast, the $C_7H_7^+$ fragment, which is associated with aromatic and hydrocarbon-like structures in α-pinene and aromatic SOA,[75] was initially low for all three VOCs and decreased with aqueous photooxidation time. This is consistent with progressive oxidation of less oxygenated hydrocarbon moieties in solutions. The $C_2H_3O^+$ and CHO^+ fragments, which are commonly associated with moderately oxidized species,[74,76] were also observed throughout the experiments. The $C_2H_3O^+$ fragment is frequently linked to carbonyl-containing compounds,[74] while CHO^+ is associated with alcohols, esters, and aldehydes.[74,76] For α-pinene and toluene aqSOA, the combined $C_2H_3O^+$ and CHO^+ signal increased during the first 60 min of aqueous photooxidation and subsequently decreased between 60 and 90 min. This behavior is consistent with the initial formation of intermediate oxygenated products followed by their further oxidation to more highly oxidized carboxylic acid-containing species. A similar trend was observed for limonene aqSOA, although the decrease in the $C_2H_3O^+$ and CHO^+ signal occurred earlier.

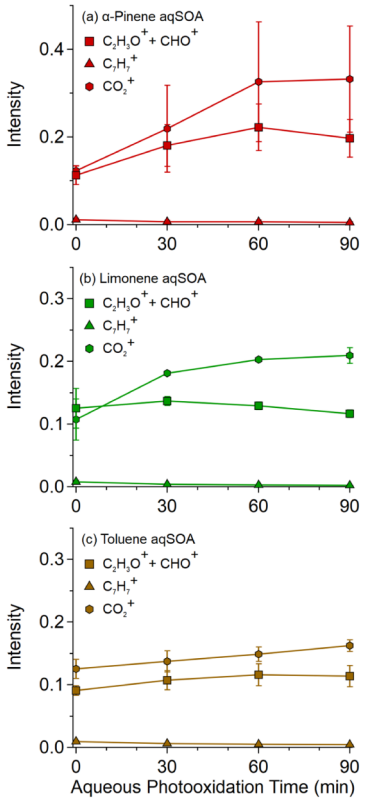

Figure 4. AMS fragments for (a) α-pinene aqSOA, (b) limonene aqSOA, and (c) toluene aqSOA over the course of aqueous-phase photooxidation. Squares represent the combined $C_2H_3O^+$ and CHO^+ fragment ions, triangles represent the $C_7H_7^+$ fragment ion, and hexagons represent the CO_2^+ fragment ion. Error bars represent one standard deviation.

The relatively large variability in several AMS fragments for α-pinene aqSOA should be considered when interpreting these temporal trends.

3.3. ESI-HRMS of α-Pinene-Derived WSOG and aqSOA

High-resolution mass spectral analysis of WSOG and aqSOA samples from the α-pinene experiments provided useful insight into the formation and depletion of intermediates and late-stage products through analysis of formula distributions. The ESI-HRMS spectra for α-pinene WSOG samples before and after aqueous-phase photooxidation are shown in Figure 5 for both ESI(−) and (+) modes. In both ESI modes, the observed aqueous-phase photooxidation products corresponded to small organic acids (C_1−C_4 compounds) and monomers (C_7−C_{10} compounds). There were essentially no ions observed above m/z 300. The ESI(−) mass spectrum was dominated by the bicarbonate ion (HCO_3^-) as well as small organic acids such $C_2H_2O_4$ (oxalic acid) and $C_2H_4O_2$ (acetic acid). The signals for these small organic acids mostly grew in relative intensity with aqueous photooxidation time (Figure 6a). Small mono- and dicarboxylic acids have been reported as main constituents of WSOGs.[2,5,12,13,44,77] The species $C_2H_2O_3$ (glyoxylic acid) and $C_2H_4O_3$ (glycolic acid) were also present and are known products of aqueous-phase photooxidation of acetic acid.[32] Highly oxidized small carboxylic acids are more stable with respect to •OH attack and thus are relatively slow to photooxidize to CO_2 compared to larger species,[78] consistent with our observations of elevated bicarbonate ion in solution. Note that the detection range of the instrument (limited to

https://doi.org/10.1021/acsestair.6c00044
ACS EST Air 2026, 3, 1811−1821

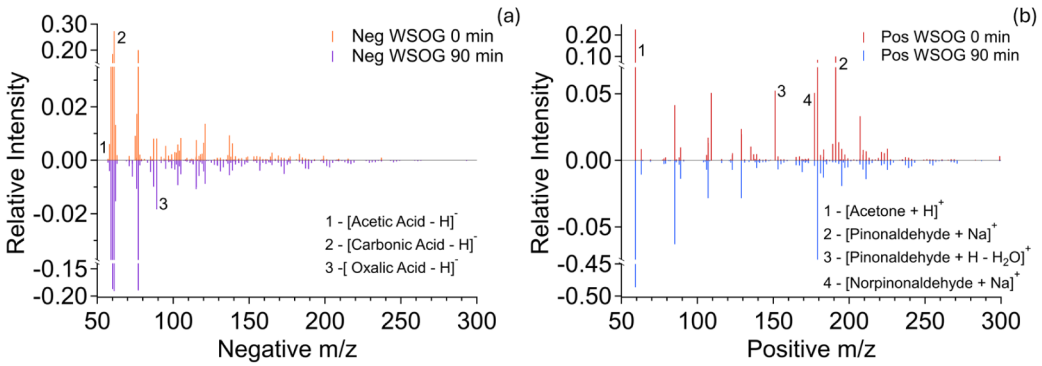

Figure 5. ESI(−) (a) and ESI(+) (b) data show the composition of α-pinene WSOGs before aqueous-phase photooxidation (0 min, orange or red) and after aqueous-phase photooxidation (90 min, purple or blue, inverted for clarity). The x-axis represents the observed m/z of the ions. Select m/z values are indicated by numbers and corresponding ion assignments. Each peak is normalized to the sum of all peaks in the sample.

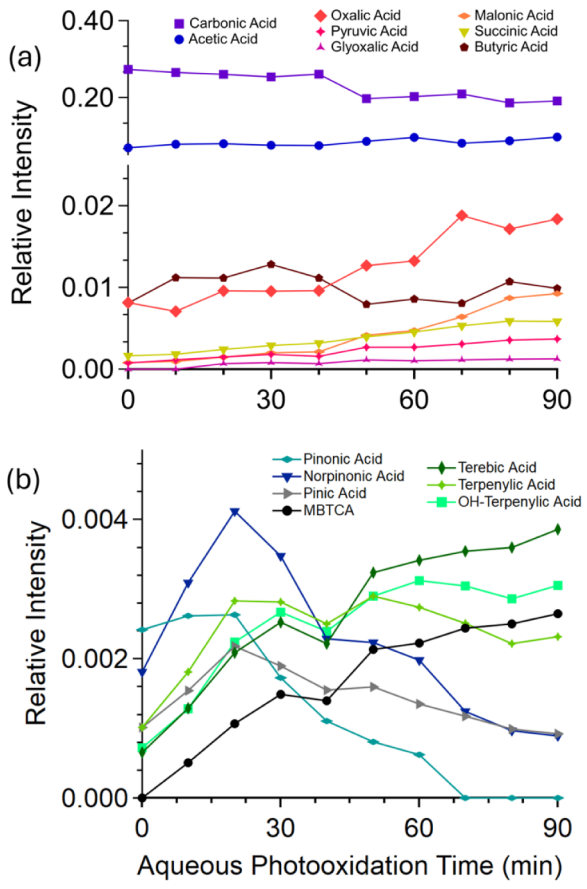

Figure 6. Individual ion relative intensities for ESI(−) over the course of aqueous-phase photooxidation. Signals from bicarbonate (labeled as "carbonic acid") and from small organic acids are shown in panel (a). The α-pinene-derived monomeric acids are shown in panel (b).

m/z > 50) prevents observation of some expected carboxylic acids such as formic acid. However, such small organic compounds have relatively high volatilities and are not expected to have contributed appreciably to particle aqSOA mass in these laboratory experiments.

Monomeric SOA products also appeared in the aqSOA samples (Figure 6b). Throughout aqueous-phase photooxidation, there was a clear decrease in $C_{10}H_{16}O_3$ (pinonic acid), a common primary product of α-pinene gas-phase oxidation. Over the same experimental time, $C_8H_{12}O_6$ (MBTCA), a known aqueous-phase oxidation product of pinonic acid[33,79] increased. Other products also increased with aqueous photooxidation time, such as $C_8H_{12}O_4$ (terpenylic acid), $C_8H_{12}O_5$ (OH-terpenylic acid), and $C_7H_{10}O_4$ (terebic acid). These compounds have sufficiently low volatilities, which contributed to the particle aqSOA mass observed in Figure 2. The predicted volatility distributions of α-pinene WSOGs at 0 and 90 min of aqueous photooxidation can be seen in Figure S6a,c, where products were predicted to have lower volatilities after aqueous-phase photooxidation.

In ESI(+) spectra (Figures 5b and 7), C_3H_6O (acetone), a known gas-phase oxidation product of α-pinene,[80−82] had the

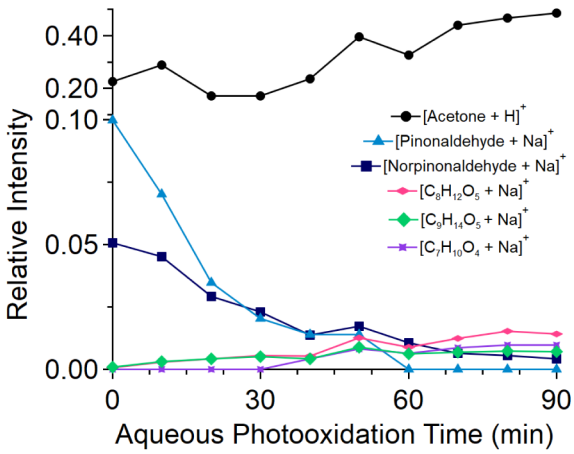

Figure 7. Individual ion relative intensities for ESI(+) over the course of aqueous-phase photooxidation. The majority of compounds are ionized as Na^+ adducts, as shown.

largest relative intensity despite its relatively low Henry's law constant of 2.5 × 10^1 M atm^{-1}.[83] In laboratory experiments, acetone has been shown to be the most abundant product of α-pinene oxidation on a per-carbon basis.[84] Similar to the small organic acids observed in ESI(−), acetone has a high volatility ($\log C_0$ = 8.3 $\mu g\ m^{-3}$; see SI section S8 for more details), preventing it from significantly contributing to the particulate aqSOA mass in these experiments. The increasing relative intensity of acetone with aqueous photooxidation time is primarily due to other peaks decreasing faster than acetone. Larger molecular weight species that contain carbonyl functional groups were abundant in ESI(+) spectra, including $C_{10}H_{16}O_2$ (pinonaldehyde), $C_{10}H_{14}O$ (pinonaldehyde that lost a water molecule in the ion source and/or myrtenal), $C_9H_{14}O_2$

https://doi.org/10.1021/acsestair.6c00044
ACS EST Air 2026, 3, 1811−1821

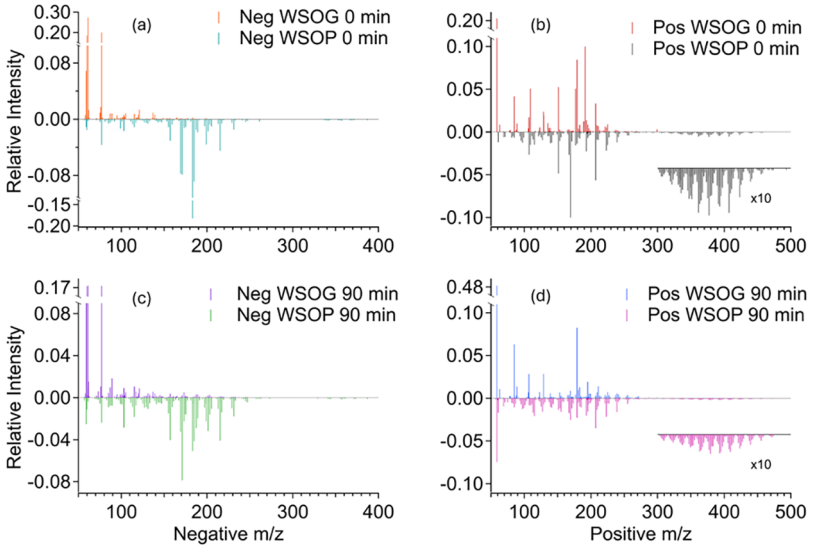

Figure 8. ESI-HRMS plots of WSOG vs WSOP samples before and after aqueous-phase photooxidation. Panels (a) and (b) show samples from 0 min, and panels (c) and (d) correspond to the 90 min photooxidation. Panels (a) and (c) are for ESI(−), and panels (b) and (d) are for ESI(+) data. WSOG samples are shown on the positive *y*-axis, while WSOP data are inverted for ease of comparison. The dimer region is magnified by a factor of 10 for the ESI(+). Each peak is normalized to the sum of all peaks in the sample.

(norpinonaldehyde), and $C_{10}H_{16}O_3$ (10-hydroxy-pinonaldehyde and/or pinonic acid). These monomeric carbonyls exhibited a prominent decrease in relative intensity at the onset of aqueous-phase photooxidation (Figure 7) and were likely precursors for the formation of observed particulate aqSOA mass (Figure 2). Additional multifunctional oxidized species, such as $C_7H_{10}O_4$, $C_8H_{12}O_5$, and $C_9H_{14}O_5$ were observed in ESI(+) spectra, and their intensity increased with aqueous photooxidation time, further demonstrating the formation of oxidized, lower volatility species present in aqSOA.

Dimeric products of monoterpene oxidation (C_{16}−C_{20}) are frequently observed above m/z 300, but such species were not identified in WSOG samples, either before or after aqueous-phase photooxidation. More concentrated aqueous solutions, such as ALW, can more readily form dimers and oligomers from organic radical−radical reactions, relative to dilute aqueous systems such as cloudwater and fogwater.[2,12,30,85] Ambient cloudwater contains larger molecular weight species in addition to smaller carboxylic acids. Ambient cloudwater samples from Colorado, USA, notably contained high relative abundances of C_{10}, C_{15}, and C_{20} compounds indicative of strong terpene influence.[40] Ambient cloudwater in Southern China also contained traces of α-pinene products.[44] Ambient cloudwater in France contained monomers, dimers, and organosulfates derived from α-pinene.[41,42] It should be noted that the detection of larger molecular weight species in cloudwater may not have originated from the uptake of the observed WSOG species but from preexisting WSOPs[41,42] that served as nuclei or were scavenged.

3.4. Comparison Between Composition of WSOGs and WSOPs

High-resolution mass spectra of WSOGs and WSOPs exhibited different trends in relative peak intensity during aqueous-phase photooxidation (Figure 8). ESI-HRMS spectra of WSOP samples demonstrated strong relative intensity signals in the monomer region of both ESI(+) and (−), more so than WSOG samples. WSOP samples also contained clear peaks in the dimer region, particularly in ESI(+) within the m/z 300−450 range. Peak-abundance m/z averages were calculated by multiplying each m/z value by its relative abundance and summing all weighted values. Peak-abundance m/z averages allow for the comparison of m/z averages between samples while accounting for the relative intensity of each peak. The peak-abundance average m/z of WSOPs decreased from m/z 169 to 163 in ESI(−) and m/z 202 to 173 in ESI(+). The peak-abundance average m/z decreases of WSOPs were due in large part to the degradation of the dimer region. Dimers produced by α-pinene gas-phase oxidation are known to efficiently degrade during aqueous-phase photooxidation and photolysis.[79,86,87] Dimers can react with •OH to form alkoxy radicals that have been shown to undergo β-scission reactions, which split the dimer into smaller molecular weight products.[79,86] Conversely, monomeric α-pinene oxidation products, such as cis-pinonic acid, preferentially functionalize in the aqueous phase rather than oligomerize,[79] which can be seen in Figure S6b, d from the increase in the O/C ratio represented by the color shift after 90 min of WSOP aqueous-phase photooxidation.

The peak-abundance average m/z of observed WSOG compounds in ESI(−) increased from m/z 76 to 83 due to the growth in monomeric species signal during aqueous-phase photooxidation. The peak-abundance average m/z in ESI(+) of observed WSOG compounds decreased from m/z 140 to 110, resulting from the depletion of higher molecular weight carbonyl and carboxylic acid species. WSOG samples experienced an increase in monomeric species (m/z 150−250) and small organic acids (m/z < 100) arising from the aqueous-phase photooxidation of carbonyl species. Lamkaddam et al. showed that there were noticeable differences between gas-phase and particle-phase products from isoprene aqueous-phase photooxidation.[23] There was a higher proportion of C_5 compounds in the particle phase, such as isoprene derivatives, while in the gas phase, there was a greater proportion of C_{2-4} compounds, likely consisting of smaller organic acids or fragments. Additionally, $C_{<10}$ isoprene oxidation products in the particle phase had more oxygens

https://doi.org/10.1021/acsestair.6c00044
ACS EST Air 2026, 3, 1811−1821

per carbon than those in the gas phase. This is because the species with more functional groups had lower volatilities, facilitating condensation into the particle phase. The results of Lamkaddam et al.[23] are consistent with the findings here, namely, the observation of smaller acids in the analysis of gas-phase products and larger, more oxygenated condensed products in the particle phase.

4. ATMOSPHERIC IMPLICATIONS

Aqueous-phase photooxidation of WSOGs derived from α-pinene gas-phase oxidation generated chemically distinct aqSOA enriched in oxygenated monomeric products. In contrast to WSOP processing, which was characterized by fragmentation and depletion of dimeric species, WSOG oxidation favored the formation of lower-volatility oxygenated products and increasing O/C ratios during aqueous-phase aging. The elevated O/C ratios of the aqSOA suggest that these particles may exhibit different hygroscopic and cloud-processing behaviors relative to less oxidized gasSOA systems. These observations suggest that aqueous transformation pathways differ substantially for dissolved gaseous oxidation products relative to preexisting particulate SOA.

The measured aqSOA yields demonstrate that cloud or ALW processing of monoterpene-derived WSOGs can contribute to atmospheric SOA formation. Applying the measured 90-min Y_2 yields to estimated global precursor emissions[52,55,88] gives approximate aqSOA production potentials of 1.3 Tg yr^{-1} for α-pinene, 0.15 Tg yr^{-1} for limonene, and 0.028 Tg yr^{-1} for toluene. Relative to an estimated global SOA source of ∼140 Tg yr^{-1},[89−91] these values correspond to potential contributions of approximately 0.9%, 0.1%, and 0.02%, respectively. These estimates represent simplified upper-bound calculations based on ∼25 h of equivalent cloud processing time and do not account for deposition, reversible partitioning, multiphase coupling, or cloud microphysical variability.

At atmospherically relevant mass concentrations, the aqSOA yields measured here were approximately an order of magnitude lower than reported gasSOA yields for α-pinene, limonene, and toluene.[92−94] However, aqueous SOA formation may still represent an important regional source under conditions with elevated liquid water content, repeated cloud processing, or persistent ALW. The results further demonstrate that WSOG uptake and aqueous-phase photooxidation can generate aqSOA with chemical compositions distinct from both gasSOA and aqSOA formed through WSOP processing, highlighting the need to better constrain multiphase processing pathways in atmospheric models.

■ ASSOCIATED CONTENT

Supporting Information

The Supporting Information is available free of charge at https://pubs.acs.org/doi/10.1021/acsestair.6c00044.

Control experiments for the OFR; diagrams for the mist chamber and aqueous-phase photooxidation setup; gas-phase oxidation in the OFR; calculation of aqueous •OH concentration using terephthalic acid and its relation to ambient exposure times; mass yield calculations; TOC measurements; volatility distributions; SMPS control measurements; factors affecting WSOG partitioning; instrument characterization settings; and cleaning protocol for equipment (PDF)

■ AUTHOR INFORMATION

Corresponding Authors

Annmarie G. Carlton − *Department of Chemistry, University of California Irvine, Irvine, California 92697, United States;* orcid.org/0000-0002-8574-1507; Email: agcarlto@uci.edu

Sergey A. Nizkorodov − *Department of Chemistry, University of California Irvine, Irvine, California 92697, United States;* orcid.org/0000-0003-0891-0052; Email: nizkorod@uci.edu

Authors

Matthew L. Zaragoza − *Department of Chemistry, University of California Irvine, Irvine, California 92697, United States;* orcid.org/0000-0003-2737-0610

Lisa M. Wingen − *Department of Chemistry, University of California Irvine, Irvine, California 92697, United States;* orcid.org/0000-0001-5847-9913

Complete contact information is available at: https://pubs.acs.org/10.1021/acsestair.6c00044

Notes

The authors declare no competing financial interest.

■ ACKNOWLEDGMENTS

This work was supported by the US National Science Foundation grants AGS-2334731 and AGS-2430367. The authors thank Avisa Charmchi, Sijia Liu, and Jackson Ryan (University of California, Irvine) for assistance with the gas chromatography−mass spectrometer. The authors also thank Dr. Veronique Perraud and Dr. Madeline Cooke (University of California, Irvine) for assistance with ESI-HRMS method development and for assistance with the PTR-MS measurements.

■ REFERENCES

(1) Hallquist, M.; Wenger, J. C.; Baltensperger, U.; Rudich, Y.; Simpson, D.; Claeys, M.; Dommen, J.; Donahue, N. M.; George, C.; Goldstein, A. H.; et al. The Formation, Properties and Impact of Secondary Organic Aerosol: Current and Emerging Issues. *Atmos. Chem. Phys.* **2009**, *9* (14), 5155−5236.

(2) Ervens, B.; Turpin, B. J.; Weber, R. J. Secondary Organic Aerosol Formation in Cloud Droplets and Aqueous Particles (aqSOA): A Review of Laboratory, Field and Model Studies. *Atmos. Chem. Phys.* **2011**, *11* (21), 11069−11102.

(3) Keene, W. C.; Galloway, J. N. Considerations Regarding Sources for Formic and Acetic Acids in the Troposphere. *J. Geophys. Res.* **1986**, *91* (D13), 14466−14474.

(4) Anderson, C. H.; Dibb, J. E.; Griffin, R. J.; Hagler, G. S. W.; Bergin, M. H. Atmospheric Water-Soluble Organic Carbon Measurements at Summit, Greenland. *Atmos. Environ.* **2008**, *42* (22), 5612−5621.

(5) Paulot, F.; Wunch, D.; Crounse, J. D.; Toon, G. C.; Millet, D. B.; De Carlo, P. F.; Vigouroux, C.; Deutscher, N. M.; González Abad, G.; Notholt, J.; Warneke, T.; Hannigan, J. W.; Warneke, C.; De Gouw, J. A.; Dunlea, E. J.; De Mazière, M.; Griffith, D. W. T.; Bernath, P.; Jimenez, J. L.; Wennberg, P. O. Importance of Secondary Sources in the Atmospheric Budgets of Formic and Acetic Acids. *Atmos. Chem. Phys.* **2011**, *11* (5), 1989−2013.

(6) Liu, J.; Zhang, X.; Parker, E. T.; Veres, P. R.; Roberts, J. M.; De Gouw, J. A.; Hayes, P. L.; Jimenez, J. L.; Murphy, J. G.; Ellis, R. A.; Huey, L. G.; Weber, R. J. On the Gas-particle Partitioning of Soluble Organic Aerosol in Two Urban Atmospheres with Contrasting

Emissions: 2. Gas and Particle Phase Formic Acid. *J. Geophys. Res.* **2012**, *117* (D21), 2012JD017912.
(7) Mungall, E. L.; Abbatt, J. P. D.; Wentzell, J. J. B.; Wentworth, G. R.; Murphy, J. G.; Kunkel, D.; Gute, E.; Tarasick, D. W.; Sharma, S.; Cox, C. J.; Uttal, T.; Liggio, J. High Gas-Phase Mixing Ratios of Formic and Acetic Acid in the High Arctic. *Atmos. Chem. Phys.* **2018**, *18* (14), 10237−10254.
(8) Legrand, M.; Preunkert, S.; Galy-Lacaux, C.; Liousse, C.; Wagenbach, D. Atmospheric Year-round Records of Dicarboxylic Acids and Sulfate at Three French Sites Located between 630 and 4360 m Elevation. *J. Geophys. Res.* **2005**, *110* (D13), 2004JD005515.
(9) Falkovich, A. H.; Graber, E. R.; Schkolnik, G.; Rudich, Y.; Maenhaut, W.; Artaxo, P. Low Molecular Weight Organic Acids in Aerosol Particles from Rondônia, Brazil, during the Biomass-Burning, Transition and Wet Periods. *Atmos. Chem. Phys.* **2005**, *5* (3), 781−797.
(10) Ervens, B. Modeling the Processing of Aerosol and Trace Gases in Clouds and Fogs. *Chem. Rev.* **2015**, *115* (10), 4157−4198.
(11) Kawamura, K.; Tachibana, E.; Okuzawa, K.; Aggarwal, S. G.; Kanaya, Y.; Wang, Z. F. High Abundances of Water-Soluble Dicarboxylic Acids, Ketocarboxylic Acids and α-Dicarbonyls in the Mountaintop Aerosols over the North China Plain during Wheat Burning Season. *Atmos. Chem. Phys.* **2013**, *13* (16), 8285−8302.
(12) Ervens, B.; Sorooshian, A.; Lim, Y. B.; Turpin, B. J. Key Parameters Controlling OH-initiated Formation of Secondary Organic Aerosol in the Aqueous Phase (aqSOA). *J. Geophys. Res.: Atmos* **2014**, *119* (7), 3997−4016.
(13) Sun, X.; Wang, Y.; Li, H.; Yang, X.; Sun, L.; Wang, X.; Wang, T.; Wang, W. Organic Acids in Cloud Water and Rainwater at a Mountain Site in Acid Rain Areas of South China. *Environ. Sci. Pollut. Res.* **2016**, *23* (10), 9529−9539.
(14) Schurman, M. I.; Boris, A.; Desyaterik, Y.; Collett, J. L., Jr. Aqueous Secondary Organic Aerosol Formation in Ambient Cloud Water Photo-Oxidations. *Aerosol Air Qual. Res.* **2018**, *18* (1), 15−25.
(15) Lawrence, C. E.; Casson, P.; Brandt, R.; Schwab, J. J.; Dukett, J. E.; Snyder, P.; Yerger, E.; Kelting, D.; VandenBoer, T. C.; Lance, S. Long-Term Monitoring of Cloud Water Chemistry at Whiteface Mountain: The Emergence of a New Chemical Regime. *Atmos. Chem. Phys.* **2023**, *23* (2), 1619−1639.
(16) Hawkins, L. N.; Russell, L. M.; Covert, D. S.; Quinn, P. K.; Bates, T. S. Carboxylic Acids, Sulfates, and Organosulfates in Processed Continental Organic Aerosol over the Southeast Pacific Ocean during VOCALS-REx 2008. *J. Geophys. Res.* **2010**, *115* (D13), 2009JD013276.
(17) Mochizuki, T.; Kawamura, K.; Miyazaki, Y.; Kunwar, B.; Boreddy, S. K. R. Distributions and Sources of Low-Molecular-Weight Monocarboxylic Acids in Gas and Particles from a Deciduous Broadleaf Forest in Northern Japan. *Atmos. Chem. Phys.* **2019**, *19* (4), 2421−2432.
(18) Kawamura, K. Geochemical Studies of Low Molecular Weight Organic Acids in the Atmosphere: Sources, Formation Pathways, and Gas/Particle Partitioning. *Proc. Jpn. Acad. Ser. B* **2023**, *99* (1), 1−28.
(19) Presto, A. A.; Huff Hartz, K. E.; Donahue, N. M. Secondary Organic Aerosol Production from Terpene Ozonolysis. 1. Effect of UV Radiation. *Environ. Sci. Technol.* **2005**, *39* (18), 7036−7045.
(20) Ng, N. L.; Kroll, J. H.; Chan, A. W. H.; Chhabra, P. S.; Flagan, R. C.; Seinfeld, J. H. Secondary Organic Aerosol Formation from *m* -Xylene, Toluene, and Benzene. *Atmos. Chem. Phys.* **2007**, *7* (14), 3909−3922.
(21) Shilling, J. E.; Chen, Q.; King, S. M.; Rosenoern, T.; Kroll, J. H.; Worsnop, D. R.; De Carlo, P. F.; Aiken, A. C.; Sueper, D.; Jimenez, J. L.; Martin, S. T. Loading-Dependent Elemental Composition of α-Pinene SOA Particles. *Atmos. Chem. Phys.* **2009**, *9* (3), 771−782.
(22) Mutzel, A.; Zhang, Y.; Böge, O.; Rodigast, M.; Kolodziejczyk, A.; Wang, X.; Herrmann, H. Importance of Secondary Organic Aerosol Formation of α-Pinene, Limonene, and m-Cresol Comparing Day- and Nighttime Radical Chemistry. *Atmos. Chem. Phys.* **2021**, *21* (11), 8479−8498.
(23) Lamkaddam, H.; Dommen, J.; Ranjithkumar, A.; Gordon, H.; Wehrle, G.; Krechmer, J.; Majluf, F.; Salionov, D.; Schmale, J.; Bjelić, S.; Carslaw, K. S.; El Haddad, I.; Baltensperger, U. Large Contribution to Secondary Organic Aerosol from Isoprene Cloud Chemistry. *Sci. Adv.* **2021**, *7* (13), No. eabe2952.
(24) Wang, T.; Li, K.; Bell, D. M.; Zhang, J.; Cui, T.; Surdu, M.; Baltensperger, U.; Slowik, J. G.; Lamkaddam, H.; El Haddad, I.; Prevot, A. S. H. Large Contribution of In-Cloud Production of Secondary Organic Aerosol from Biomass Burning Emissions. *Npj Clim Atmos Sci.* **2024**, *7* (1), 149.
(25) Faust, J. A.; Wong, J. P. S.; Lee, A. K. Y.; Abbatt, J. P. D. Role of Aerosol Liquid Water in Secondary Organic Aerosol Formation from Volatile Organic Compounds. *Environ. Sci. Technol.* **2017**, *51* (3), 1405−1413.
(26) Carlton, A. G.; Turpin, B. J.; Lim, H.; Altieri, K. E.; Seitzinger, S. Link between Isoprene and Secondary Organic Aerosol (SOA): Pyruvic Acid Oxidation Yields Low Volatility Organic Acids in Clouds. *Geophys. Res. Lett.* **2006**, *33* (6), 2005GL025374.
(27) Guzmán, M. I.; Colussi, A. J.; Hoffmann, M. R. Photoinduced Oligomerization of Aqueous Pyruvic Acid. *J. Phys. Chem. A* **2006**, *110* (10), 3619−3626.
(28) Carlton, A. G.; Turpin, B. J.; Altieri, K. E.; Seitzinger, S.; Reff, A.; Lim, H.-J.; Ervens, B. Atmospheric Oxalic Acid and SOA Production from Glyoxal: Results of Aqueous Photooxidation Experiments. *Atmos. Environ.* **2007**, *41* (35), 7588−7602.
(29) Altieri, K. E.; Seitzinger, S. P.; Carlton, A. G.; Turpin, B. J.; Klein, G. C.; Marshall, A. G. Oligomers Formed through In-Cloud Methylglyoxal Reactions: Chemical Composition, Properties, and Mechanisms Investigated by Ultra-High Resolution FT-ICR Mass Spectrometry. *Atmos. Environ.* **2008**, *42* (7), 1476−1490.
(30) Lim, Y. B.; Tan, Y.; Perri, M. J.; Seitzinger, S. P.; Turpin, B. J. Aqueous Chemistry and Its Role in Secondary Organic Aerosol (SOA) Formation. *Atmos. Chem. Phys.* **2010**, *10* (21), 10521−10539.
(31) Ortiz-Montalvo, D. L.; Lim, Y. B.; Perri, M. J.; Seitzinger, S. P.; Turpin, B. J. Volatility and Yield of Glycolaldehyde SOA Formed through Aqueous Photochemistry and Droplet Evaporation. *Aerosol Sci. Technol.* **2012**, *46* (9), 1002−1014.
(32) Tan, Y.; Lim, Y. B.; Altieri, K. E.; Seitzinger, S. P.; Turpin, B. J. Mechanisms Leading to Oligomers and SOA through Aqueous Photooxidation: Insights from OH Radical Oxidation of Acetic Acid and Methylglyoxal. *Atmos. Chem. Phys.* **2012**, *12* (2), 801−813.
(33) Aljawhary, D.; Zhao, R.; Lee, A. K. Y.; Wang, C.; Abbatt, J. P. D. K. Mechanism, and Secondary Organic Aerosol Yield of Aqueous Phase Photo-Oxidation of α-Pinene Oxidation Products. *J. Phys. Chem. A* **2016**, *120* (9), 1395−1407.
(34) Witkowski, B.; Gierczak, T. Characterization of the Limonene Oxidation Products with Liquid Chromatography Coupled to the Tandem Mass Spectrometry. *Atmos. Environ.* **2017**, *154*, 297−307.
(35) Witkowski, B.; Gierczak, T. *Cis*- Pinonic Acid Oxidation by Hydroxyl Radicals in the Aqueous Phase under Acidic and Basic Conditions: Kinetics and Mechanism. *Environ. Sci. Technol.* **2017**, *51* (17), 9765−9773.
(36) Witkowski, B.; Jurdana, S.; Gierczak, T. Limononic Acid Oxidation by Hydroxyl Radicals and Ozone in the Aqueous Phase. *Environ. Sci. Technol.* **2018**, *52* (6), 3402−3411.
(37) Amorim, J. V.; Guo, X.; Gautam, T.; Fang, R.; Fotang, C.; Williams, F. J.; Zhao, R. Photo-Oxidation of Pinic Acid in the Aqueous Phase: A Mechanistic Investigation under Acidic and Basic pH Conditions. *Environ. Sci.: Atmos* **2021**, *1* (5), 276−287.
(38) Lee, A. K. Y.; Herckes, P.; Leaitch, W. R.; Macdonald, A. M.; Abbatt, J. P. D. Aqueous OH Oxidation of Ambient Organic Aerosol and Cloud Water Organics: Formation of Highly Oxidized Products: Aqueous Oxidation of Ambient Organics. *Geophys. Res. Lett.* **2011**, *38* (11), n/a−n/a.
(39) Sareen, N.; Carlton, A. G.; Surratt, J. D.; Gold, A.; Lee, B.; Lopez-Hilfiker, F. D.; Mohr, C.; Thornton, J. A.; Zhang, Z.; Lim, Y. B.; Turpin, B. J. Identifying Precursors and Aqueous Organic Aerosol Formation Pathways during the SOAS Campaign. *Atmos. Chem. Phys.* **2016**, *16* (22), 14409−14420.

https://doi.org/10.1021/acsestair.6c00044
ACS EST Air 2026, 3, 1811−1821

(40) Zhao, Y.; Hallar, A. G.; Mazzoleni, L. R. Atmospheric Organic Matter in Clouds: Exact Masses and Molecular Formula Identification Using Ultrahigh-Resolution FT-ICR Mass Spectrometry. *Atmos. Chem. Phys.* **2013**, *13* (24), 12343−12362.
(41) Bianco, A.; Deguillaume, L.; Vaïtilingom, M.; Nicol, E.; Baray, J.-L.; Chaumerliac, N.; Bridoux, M. Molecular Characterization of Cloud Water Samples Collected at the Puy de Dôme (France) by Fourier Transform Ion Cyclotron Resonance Mass Spectrometry. *Environ. Sci. Technol.* **2018**, *52* (18), 10275−10285.
(42) Bianco, A.; Riva, M.; Baray, J.-L.; Ribeiro, M.; Chaumerliac, N.; George, C.; Bridoux, M.; Deguillaume, L. Chemical Characterization of Cloudwater Collected at Puy de Dôme by FT-ICR MS Reveals the Presence of SOA Components. *ACS Earth Space Chem.* **2019**, *3* (10), 2076−2087.
(43) Cook, R. D.; Lin, Y.-H.; Peng, Z.; Boone, E.; Chu, R. K.; Dukett, J. E.; Gunsch, M. J.; Zhang, W.; Tolic, N.; Laskin, A.; Pratt, K. A. B. Urban, and Wildfire Influences on the Molecular Composition of Dissolved Organic Compounds in Cloud Water. *Atmos. Chem. Phys.* **2017**, *17* (24), 15167−15180.
(44) Sun, W.; Fu, Y.; Zhang, G.; Yang, Y.; Jiang, F.; Lian, X.; Jiang, B.; Liao, Y.; Bi, X.; Chen, D.; Chen, J.; Wang, X.; Ou, J.; Peng, P.; Sheng, G. Measurement Report: Molecular Characteristics of Cloud Water in Southern China and Insights into Aqueous-Phase Processes from Fourier Transform Ion Cyclotron Resonance Mass Spectrometry. *Atmos. Chem. Phys.* **2021**, *21* (22), 16631−16644.
(45) Akimoto, H.; Hirokawa, J.; *Atmospheric Multiphase Chemistry: fundamentals of Secondary Aerosol Formation*, 1st ed.; Wiley, 2020; .
(46) Bianco, A.; Passananti, M.; Brigante, M.; Mailhot, G. Photochemistry of the Cloud Aqueous Phase: A Review. *Molecules* **2020**, *25* (2), 423.
(47) Ervens, B. Average Cloud Droplet Size and Composition: Good Assumptions for Predicting Oxidants in the Atmospheric Aqueous Phase? *J. Phys. Chem. A* **2022**, *126* (44), 8295−8304.
(48) Nguyen, T. K. V.; Zhang, Q.; Jimenez, J. L.; Pike, M.; Carlton, A. G. Liquid Water: Ubiquitous Contributor to Aerosol Mass. *Environ. Sci. Technol. Lett.* **2016**, *3* (7), 257−263.
(49) Carlton, A. G.; Turpin, B. J. Particle Partitioning Potential of Organic Compounds Is Highest in the Eastern US and Driven by Anthropogenic Water. *Atmos. Chem. Phys.* **2013**, *13* (20), 10203−10214.
(50) Herrmann, H.; Schaefer, T.; Tilgner, A.; Styler, S. A.; Weller, C.; Teich, M.; Otto, T. Tropospheric Aqueous-Phase Chemistry: Kinetics, Mechanisms, and Its Coupling to a Changing Gas Phase. *Chem. Rev.* **2015**, *115* (10), 4259−4334.
(51) Sapkota, S.; Shekhar, P.; Murphy, B.; Pye, H. O. T.; Hennigan, C. J.; El-Sayed, M. M. H. Seasonal Assessment of Secondary Organic Aerosol Formed through Aqueous Pathways in the Eastern United States. *ACS Earth Space Chem.* **2025**, *9* (4), 876−887.
(52) Guenther, A. B.; Jiang, X.; Heald, C. L.; Sakulyanontvittaya, T.; Duhl, T.; Emmons, L. K.; Wang, X. The Model of Emissions of Gases and Aerosols from Nature Version 2.1 (MEGAN2.1): An Extended and Updated Framework for Modeling Biogenic Emissions. *Geosci. Model Dev.* **2012**, *5* (6), 1471−1492.
(53) Karl, T.; Apel, E.; Hodzic, A.; Riemer, D. D.; Blake, D. R.; Wiedinmyer, C. Emissions of Volatile Organic Compounds Inferred from Airborne Flux Measurements over a Megacity. *Atmos. Chem. Phys.* **2009**, *9* (1), 271−285.
(54) Barletta, B.; Meinardi, S.; Sherwood Rowland, F.; Chan, C.-Y.; Wang, X.; Zou, S.; Yin Chan, L.; Blake, D. R. Volatile Organic Compounds in 43 Chinese Cities. *Atmos. Environ.* **2005**, *39* (32), 5979−5990.
(55) Cabrera-Perez, D.; Taraborrelli, D.; Sander, R.; Pozzer, A. Global Atmospheric Budget of Simple Monocyclic Aromatic Compounds. *Atmos. Chem. Phys.* **2016**, *16* (11), 6931−6947.
(56) Cofer, W. R.; Collins, V. G.; Talbot, R. W. Improved Aqueous Scrubber for Collection of Soluble Atmospheric Trace Gases. *Environ. Sci. Technol.* **1985**, *19* (6), 557−560.
(57) Spaulding, R. S.; Talbot, R. W.; Charles, M. J. Optimization of a Mist Chamber (Cofer Scrubber) for Sampling Water-Soluble Organics in Air. *Environ. Sci. Technol.* **2002**, *36* (8), 1798−1808.
(58) Veghte, D. P.; China, S.; Weis, J.; Lin, P.; Hinks, M. L.; Kovarik, L.; Nizkorodov, S. A.; Gilles, M. K.; Laskin, A. Heating-Induced Transformations of Atmospheric Particles: Environmental Transmission Electron Microscopy Study. *Anal. Chem.* **2018**, *90* (16), 9761−9768.
(59) Carter, L.; Kayatin, M.; Perry, J.; Agui, J.; Green, R.; Gentry, G.; Bowman, E.; Wilson, M.; Rector, T. *Design And Delivery Of a Filter For Removal Of Siloxanes From The ISS Atmosphere*, 2016. https://ntrs.nasa.gov/api/citations/20160009721/downloads/20160009721.pdf.
(60) Hennigan, C. J.; El-Sayed, M. M. H.; Hodzic, A. Detailed Characterization of a Mist Chamber for the Collection of Water-Soluble Organic Gases. *Atmos. Environ.* **2018**, *188*, 12−17.
(61) Romonosky, D. E.; Laskin, A.; Laskin, J.; Nizkorodov, S. A. High-Resolution Mass Spectrometry and Molecular Characterization of Aqueous Photochemistry Products of Common Types of Secondary Organic Aerosols. *J. Phys. Chem. A* **2015**, *119* (11), 2594−2606.
(62) Yang, Z.; Du, L.; Li, Y.; Ge, X. Secondary Organic Aerosol Formation from Monocyclic Aromatic Hydrocarbons: Insights from Laboratory Studies. *Environ. Sci.: Processes Impacts* **2022**, *24* (3), 351−379.
(63) Loeffler, K. W.; Koehler, C. A.; Paul, N. M.; De Haan, D. O. Oligomer Formation in Evaporating Aqueous Glyoxal and Methyl Glyoxal Solutions. *Environ. Sci. Technol.* **2006**, *40* (20), 6318−6323.
(64) Yasmeen, F.; Sauret, N.; Gal, J.-F.; Maria, P.-C.; Massi, L.; Maenhaut, W.; Claeys, M. Characterization of Oligomers from Methylglyoxal under Dark Conditions: A Pathway to Produce Secondary Organic Aerosol through Cloud Processing during Nighttime. *Atmos. Chem. Phys.* **2010**, *10* (8), 3803−3812.
(65) Sui, X.; Zhou, Y.; Zhang, F.; Chen, J.; Zhu, Z.; Yu, X.-Y. Deciphering the Aqueous Chemistry of Glyoxal Oxidation with Hydrogen Peroxide Using Molecular Imaging. *Phys. Chem. Chem. Phys.* **2017**, *19* (31), 20357−20366.
(66) Zhang, F.; Yu, X.; Chen, J.; Zhu, Z.; Yu, X.-Y. Dark Air−Liquid Interfacial Chemistry of Glyoxal and Hydrogen Peroxide. *Npj Clim Atmos Sci.* **2019**, *2* (1), 28.
(67) Zhang, F.; Nguyen, M. T.; Fu, Y.; Yu, X.-Y. Interfacial Dark Aging Is an Overlooked Source of Aqueous Secondary Organic Aerosol. *Atmosphere* **2022**, *13* (2), 188.
(68) Lee, A. K. Y.; Hayden, K. L.; Herckes, P.; Leaitch, W. R.; Liggio, J.; Macdonald, A. M.; Abbatt, J. P. D. Characterization of Aerosol and Cloud Water at a Mountain Site during WACS 2010: Secondary Organic Aerosol Formation through Oxidative Cloud Processing. *Atmos. Chem. Phys.* **2012**, *12* (15), 7103−7116.
(69) Ervens, B.; Carlton, A. G.; Turpin, B. J.; Altieri, K. E.; Kreidenweis, S. M.; Feingold, G. Secondary Organic Aerosol Yields from Cloud-processing of Isoprene Oxidation Products. *Geophys. Res. Lett.* **2008**, *35* (2), 2007GL031828.
(70) Kroll, J. H.; Donahue, N. M.; Jimenez, J. L.; Kessler, S. H.; Canagaratna, M. R.; Wilson, K. R.; Altieri, K. E.; Mazzoleni, L. R.; Wozniak, A. S.; Bluhm, H.; Mysak, E. R.; Smith, J. D.; Kolb, C. E.; Worsnop, D. R. Carbon Oxidation State as a Metric for Describing the Chemistry of Atmospheric Organic Aerosol. *Nat. Chem.* **2011**, *3* (2), 133−139.
(71) Lambe, A. T.; Ahern, A. T.; Williams, L. R.; Slowik, J. G.; Wong, J. P. S.; Abbatt, J. P. D.; Brune, W. H.; Ng, N. L.; Wright, J. P.; Croasdale, D. R.; Worsnop, D. R.; Davidovits, P.; Onasch, T. B. Characterization of Aerosol Photooxidation Flow Reactors: Heterogeneous Oxidation, Secondary Organic Aerosol Formation and Cloud Condensation Nuclei Activity Measurements. *Atmos. Meas. Technol.* **2011**, *4* (3), 445−461.
(72) Zhao, D. F.; Kaminski, M.; Schlag, P.; Fuchs, H.; Acir, I.-H.; Bohn, B.; Häseler, R.; Kiendler-Scharr, A.; Rohrer, F.; Tillmann, R.; Wang, M. J.; Wegener, R.; Wildt, J.; Wahner, A.; Mentel, T. F. Secondary Organic Aerosol Formation from Hydroxyl Radical

Oxidation and Ozonolysis of Monoterpenes. *Atmos. Chem. Phys.* **2015**, *15* (2), 991−1012.
(73) Docherty, K. S.; Corse, E. W.; Jaoui, M.; Offenberg, J. H.; Kleindienst, T. E.; Krug, J. D.; Riedel, T. P.; Lewandowski, M. Trends in the Oxidation and Relative Volatility of Chamber-Generated Secondary Organic Aerosol. *Aerosol Sci. Technol.* **2018**, *52* (9), 992−1004.
(74) Yazdani, A.; Dudani, N.; Takahama, S.; Bertrand, A.; Prévôt, A. S. H.; El Haddad, I.; Dillner, A. M. Fragment Ion−Functional Group Relationships in Organic Aerosols Using Aerosol Mass Spectrometry and Mid-Infrared Spectroscopy. *Atmos. Meas. Technol.* **2022**, *15* (9), 2857−2874.
(75) Ng, N. L.; Canagaratna, M. R.; Jimenez, J. L.; Zhang, Q.; Ulbrich, I. M.; Worsnop, D. R. Real-Time Methods for Estimating Organic Component Mass Concentrations from Aerosol Mass Spectrometer Data. *Environ. Sci. Technol.* **2011**, *45* (3), 910−916.
(76) Canagaratna, M. R.; Jimenez, J. L.; Kroll, J. H.; Chen, Q.; Kessler, S. H.; Massoli, P.; Hildebrandt Ruiz, L.; Fortner, E.; Williams, L. R.; Wilson, K. R.; Surratt, J. D.; Donahue, N. M.; Jayne, J. T.; Worsnop, D. R. Elemental Ratio Measurements of Organic Compounds Using Aerosol Mass Spectrometry: Characterization, Improved Calibration, and Implications. *Atmos. Chem. Phys.* **2015**, *15* (1), 253−272.
(77) Ervens, B.; Wang, Y.; Eagar, J.; Leaitch, W. R.; Macdonald, A. M.; Valsaraj, K. T.; Herckes, P. Dissolved Organic Carbon (DOC) and Select Aldehydes in Cloud and Fog Water: The Role of the Aqueous Phase in Impacting Trace Gas Budgets. *Atmos. Chem. Phys.* **2013**, *13* (10), 5117−5135.
(78) Vel Leitner, N. K.; Dore, M. Hydroxyl Radical Induced Decomposition of Aliphatic Acids in Oxygenated and Deoxygenated Aqueous Solutions. *J. Photochem. Photobiol., A* **1996**, *99* (2−3), 137−143.
(79) Witkowski, B.; Al-Sharafi, M.; Błaziak, K.; Gierczak, T. Aging of α-Pinene Secondary Organic Aerosol by Hydroxyl Radicals in the Aqueous Phase: Kinetics and Products. *Environ. Sci. Technol.* **2023**, *57* (15), 6040−6051.
(80) Vereecken, L.; Peeters, J. Theoretical Study of the Formation of Acetone in the OH-Initiated Atmospheric Oxidation of α-Pinene. *J. Phys. Chem. A* **2000**, *104* (47), 11140−11146.
(81) Vanhees, I.; Van Den Bergh, V.; Schildermans, R.; De Boer, R.; Compernolle, F.; Vinckier, C. Determination of the Oxidation Products of the Reaction between α-Pinene and Hydroxyl Radicals by High-Performance Liquid Chromatography. *J. Chromatogr. A* **2001**, *915* (1−2), 75−83.
(82) Wisthaler, A.; Jensen, N. R.; Winterhalter, R.; Lindinger, W.; Hjorth, J. Measurements of Acetone and Other Gas Phase Product Yields from the OH-Initiated Oxidation of Terpenes by Proton-Transfer-Reaction Mass Spectrometry (PTR-MS). *Atmos. Environ.* **2001**, *35* (35), 6181−6191.
(83) Sander, R. Compilation of Henry's Law Constants (Version 5.0.0) for Water as Solvent. *Atmos. Chem. Phys.* **2023**, *23* (19), 10901−12440.
(84) Isaacman-VanWertz, G.; Massoli, P.; O'Brien, R.; Lim, C.; Franklin, J. P.; Moss, J. A.; Hunter, J. F.; Nowak, J. B.; Canagaratna, M. R.; Misztal, P. K. Chemical evolution of atmospheric organic carbon over multiple generations of oxidation. *Nature Chem.* **2018**, *10* (4), 462−468.
(85) Tan, Y.; Carlton, A. G.; Seitzinger, S. P.; Turpin, B. J. SOA from Methylglyoxal in Clouds and Wet Aerosols: Measurement and Prediction of Key Products. *Atmos. Environ.* **2010**, *44* (39), 5218−5226.
(86) Zhao, R.; Aljawhary, D.; Lee, A. K. Y.; Abbatt, J. P. D. Rapid Aqueous-Phase Photooxidation of Dimers in the α-Pinene Secondary Organic Aerosol. *Environ. Sci. Technol. Lett.* **2017**, *4* (6), 205−210.
(87) Klodt, A. L.; Romonosky, D. E.; Lin, P.; Laskin, J.; Laskin, A.; Nizkorodov, S. A. Aqueous Photochemistry of Secondary Organic Aerosol of α-Pinene and α-Humulene in the Presence of Hydrogen Peroxide or Inorganic Salts. *ACS Earth Space Chem.* **2019**, *3* (12), 2736−2746.
(88) Sindelarova, K.; Granier, C.; Bouarar, I.; Guenther, A.; Tilmes, S.; Stavrakou, T.; Müller, J.-F.; Kuhn, U.; Stefani, P.; Knorr, W. Global Data Set of Biogenic VOC Emissions Calculated by the MEGAN Model over the Last 30 Years. *Atmos. Chem. Phys.* **2014**, *14* (17), 9317−9341.
(89) Hodzic, A.; Kasibhatla, P. S.; Jo, D. S.; Cappa, C. D.; Jimenez, J. L.; Madronich, S.; Park, R. J. Rethinking the Global Secondary Organic Aerosol (SOA) Budget: Stronger Production, Faster Removal, Shorter Lifetime. *Atmos. Chem. Phys.* **2016**, *16* (12), 7917−7941.
(90) Tilmes, S.; Hodzic, A.; Emmons, L. K.; Mills, M. J.; Gettelman, A.; Kinnison, D. E.; Park, M.; Lamarque, J.; Vitt, J. F.; Shrivastava, M.; Campuzano-Jost, P.; Jimenez, J. L.; Liu, J. L. X. Climate Forcing and Trends of Organic Aerosols in the Community Earth System Model (CESM2). *J. Adv. Model Earth Syst.* **2019**, *11* (12), 4323−4351.
(91) Spracklen, D. V.; Jimenez, J. L.; Carslaw, K. S.; Worsnop, D. R.; Evans, M. J.; Mann, G. W.; Zhang, Q.; Canagaratna, M. R.; Allan, J.; Coe, H.; McFiggans, G.; Rap, A.; Forster, P. Aerosol Mass Spectrometer Constraint on the Global Secondary Organic Aerosol Budget. *Atmos. Chem. Phys.* **2011**, *11* (23), 12109−12136.
(92) Henry, K. M.; Lohaus, T.; Donahue, N. M. Organic Aerosol Yields from α-Pinene Oxidation: Bridging the Gap between First-Generation Yields and Aging Chemistry. *Environ. Sci. Technol.* **2012**, *46* (22), 12347−12354.
(93) Mutzel, A.; Zhang, Y.; Böge, O.; Rodigast, M.; Kolodziejczyk, A.; Wang, X.; Herrmann, H. Importance of Secondary Organic Aerosol Formation of α -Pinene, Limonene, and *m* -Cresol Comparing Day- and Nighttime Radical Chemistry. *Atmos. Chem. Phys.* **2021**, *21* (11), 8479−8498.
(94) Barsanti, K. C.; Carlton, A. G.; Chung, S. H. Analyzing Experimental Data and Model Parameters: Implications for Predictions of SOA Using Chemical Transport Models. *Atmos. Chem. Phys.* **2013**, *13* (23), 12073−12088.

https://doi.org/10.1021/acsestair.6c00044
ACS EST Air 2026, 3, 1811−1821